Proceedings of ASME Turbo Expo 2011
GT2011
June 6-10, 2011, Vancouver, British Columbia, Canada

GT2011-46402

EXPERIMENTAL INVESTIGATION ON LEAKAGE LOSS AND HEAT TRANSFER IN A STRAIGHT THROUGH LABYRINTH SEAL

Mirko Micio *, **Bruno Facchini, Luca Innocenti, Francesco Simonetti**
Energy Engineering Department "S.Stecco"
University of Florence
50139, via S.Marta 3, Florence, Italy
Tel: (+39)0554796618, Fax: (+39)0554796342
Email: mirko.micio@htc.de.unifi.it

ABSTRACT

Labyrinth seals are extensively used in turbomachinery to prevent high pressure gas from flowing into a region of low pressure. Because of thermal expansions and centrifugal forces, the actual seal clearance can vary based on engine conditions. Pressure ratio, Reynolds number, tip geometry, and seal clearance all affected the sealing performance.

This paper deals with its influence on the leakage flow and heat transfer coefficient through a thirteen teeth straight through labyrinth seal. Three gaps were experimentally investigated using a stationary test rig. The experiments covered a range of Reynolds numbers between 5000 and 50000 and pressure ratios between 1.0 and 2.7.

Cavity pressure measurements along the seal were also performed in order to characterize each constriction. In addition, 2D PIV measurements were made on the plane containing the seal teeth to obtain a high local resolution of the velocity distribution and the flow field within the seal.

Experimental results show a strong influence of clearance on both leakage loss and heat transfer as well as on the development of the flow fields. A simplified model to calculate the leakage mass flow rate is presented and validated comparing its prediction capability with experimental data. In order to improve the agreement between numerical and experimental results a correction of published correlations is proposed.

NOMENCLATURE

A	area	$[m^2]$
B	test section width	$[m]$
c	velocity	$[m \cdot s^{-1}]$
Cd	discharge coefficient	$[-]$
cl	clearance	$[mm]$
H	tooth height	$[mm]$
htc	heat transfer coefficient	$[W \cdot m^{-2} \cdot K^{-1}]$
k	conductivity	$[W \cdot m^{-1} \cdot K^{-1}]$
L	pitch	$[mm]$
$\dot{m}$	mass flow rate	$[kg \cdot s^{-1}]$
M	Mach number	$[-]$
n	number of teeth	$[-]$
Nu	Nusselt number	$[-]$
P	static pressure	$[Pa]$
R	specific gas constant	$[J \cdot kg^{-1} \cdot K^{-1}]$
Re	Reynolds number	$[-]$
t	tip tooth thickness	$[mm]$
T	static temperature	$[K]$

Subscripts

ideal	ideal condition
i	related to i-th tooth
t	total value

*Address all correspondence to this author.

theo	theoretical value	
tot	from seal inlet to seal outlet	

Greeks

α	thermal diffusivity	$[m^2 \cdot s^{-1}]$
β	pressure ratio	$[-]$
γ	specific heat ratio	$[-]$
μ	carry-over factor	$[-]$
θ	tooth angle	$[°]$
Θ	time	$[s]$

INTRODUCTION

Despite advanced sealing techniques such as brush or honeycomb seals, labyrinth seals remain the most important and widely used sealing element in turbomachines.

In order to correctly estimate the mass flow rate through the seal, it is necessary to understand well the dissipation mechanisms of energy of the flow within the seal. In the case of labyrinth seals, this energy dissipation is achieved by a combination of constrictions and cavities. When the fluid flows through the constriction (under each tooth), a part of the pressure head is converted into kinetic energy, which is dissipated through small scale turbulence-viscosity interaction in the cavity that follows. This increases the resistance to flow compared to a smooth channel and hence reduces the leakage rate.

A leakage flow equation can be developed by considering the seal as a series of orifices and cavities. The mass flow rate is represented as a function of the discharge coefficient under each tooth and the carry-over coefficient inside each cavity. The carry-over coefficient accounts for the turbulent dissipation of kinetic energy entering into each individual cavity. In other words, a higher value of carry-over coefficient indicates that the cavity is less effective in dissipating kinetic energy.

A straight through labyrinth seal is commonly used for turbines and compressors primarily due to the ease of manufacture and assembly. This design, however, has a greater kinetic energy carry-over than some other types of labyrinth seals. Hence it becomes extremely important to define the carry-over coefficient of straight through labyrinth seals in order to improve the accuracy in leakage prediction.

The theoretical flow passing through a single throttling can be calculated by applying St. Venant equation [1].

The development of a labyrinth seal leakage rate prediction equation was of interest as early as 1908 when Martin [2] presented a model. This equation, which is applicable only to incompressible flows, was based on a purely analytical approach. Whereas the St. Venant equation applied to a single constriction and therefore required an iterative algorithm to calculate the leakage through multiple blades, Martin's Equation offers a single-step procedure to determine the flow-rate. This means that intermediate pressures in the seal's cavities are not implicitly calculated by this equation.

Egli [1] provided a rational theoretical treatment of the labyrinth problem based on the flow characteristics typical for a sharp edged orifice. He identified the need for a kinetic energy carry-over coefficient suggesting that after each throttling, a small part of the kinetic energy of the steam jet will be reconverted into pressure energy, a second part will be destroyed and transferred into heat, and the remaining kinetic energy will enter the following throttling. Egli modified the basic equation put forth by Martin by including an experimentally determined flow coefficient to account for the kinetic energy carry-over. Egli also reasoned that the carry-over coefficient should increase with an increase in clearance and decrease as the axial distance between blades (tooth pitch) increases.

Hodkinson [3] modified Egli's approach to provide a semi empirical relation that was based on assumptions of a gas jet's geometry. He assumed that the fluid jet expands conically from the tip of an upstream tooth at a small angle. Vermes [4] developed an expression for the kinetic energy carry-over based upon the boundary layer theory and combined this factor with Martin's leakage equation.

Neumann, as reported by Eldin [5], developed an empirical leakage expression applicable to each constriction using the semi-empirical correlation proposed by Chaplygin for the flow coefficient.

Zimmerman and Wolf [6] examined the flow through straight-through labyrinth seals and presented a calculation method for leakage, which treated the first constriction separately. Since the carry-over effect is not present in the case of the first constriction, their method applies the St. Venant equation to the first constriction, and then applies Martin's equation, with a carry-over coefficient, to the remainder of the seal. Moreover, Zimmerman and Wolf show how a seemingly anomalous result can be obtained when the pressure in the second cavity exceeds that in the first. This is explained by the idea that in the case of a large clearance, the vena contracta (the narrowest point of the carry-over jet) in a cavity can occur well into the cavity, causing a re-diffusion effect in the second cavity, which raises the pressure of the second cavity. Zimmerman and Wolf's experimental data demonstrate this phenomenon.

Few publications dealing with the heat transfer in labyrinth seals are available in literature and only a small part provides more detailed investigations of the distribution of the local heat transfer coefficients like Metzger et al. [7] and Willenborg et al. [8, 9].

The main objective of the present study is to analyze the influence of Reynolds number, pressure ratio, and seal clearance on the discharge behavior and the heat transfer of a nonrotating straight through labyrinth seal. Data obtained in nonrotating models can be corrected for rotational effects by applying the results of Waschka et al. [10] when the circumferential velocity exceeds the axial velocity and rotational effects can no longer be neglected.

EXPERIMENTAL APPARATUS AND PROCEDURES

The labyrinth seal test rig

The flow function of the labyrinth seals is measured using the labyrinth seal test rig located at the Energetic Department Laboratory at the University of Florence. The test rig (see figure 1) consists of an open-loop suction type wind tunnel which allows pressure loss and heat transfer measurements on several seal geometries.

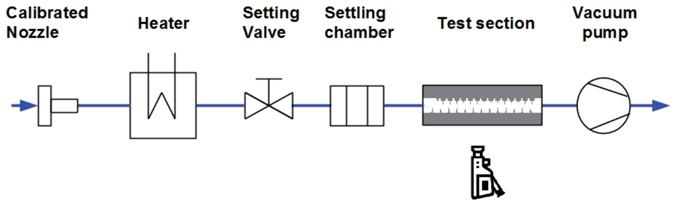

Figure 1. Schematic of the test rig

The mainstream air, at atmospheric pressure and ambient temperature, is metered through a calibrated nozzle and supplied to a 24.0 kW electronically controlled electric heater, where the desired temperature is reached and kept constant. Then it passes through a setting valve and finally enters in the test section. Four rotary vane vacuum pumps (total power installed 59.0 kW) provide the suction for a maximum mass flow rate of 0.50 kg/s. The flow rates are set up by guiding the motor speeds between 300 and 1200 rpm; the air temperature exiting from the heater is controlled by means of a four wire resistance temperature detector (RTD Pt-100).

A pressure scanner Scanivalve® DSA 3217 with temperature compensated piezoresistive relative pressure sensors allows the measurement of total or static pressure in 16 different locations with an accuracy of 6.9 Pa.

Concerning to temperature measurements, several T type thermocouples are connected to a data acquisition/switch unit (HP/Agilent® 34970A); an external reference junction has been employed. The thermocouples recovery factor, measured by means of a calibration test, has been evaluated as 0.68 and it has then been employed for the evaluation of air total temperature T_{tot} and adiabatic wall temperature T_{aw} using a recovery factor of 0.89. Thermochromic liquid crystals (TLC) are the devices used to evaluate the surface temperature T_w of the flat wall between the tooth.

A detailed error analysis yielded values of the uncertainty in the measurement of the gas mass flow was below 8%. Results deviated less than 4 percent from different sets of data which were acquired over a period of several months. Based on a one-dimensional error analysis the maximum uncertainty of the local Nusselt numbers was computed to be in the range from 12-25 percent.

The geometry of the straight through labyrinth seal with thirteen teeth investigated in the present study is shown in Figure (2). This figure shows the positions (red arrows) and the referring number of each pressure tap as well as the nomenclature used in this paper. Two thermocouples (located at position 1 and 14), normal to the flow, acquire mainstream recovery temperature.

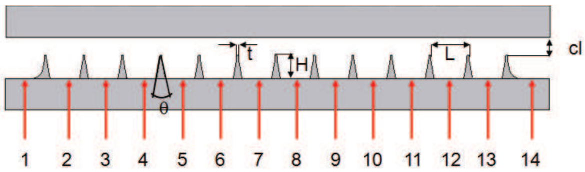

Figure 2. Labyrinth seal geometry

The pitch of the labyrinth seal is L=29.4 mm and is operated at three different clearance gaps cl=3.0 mm, 4.5 mm and 6.0 mm. The tooth tip thickness is t=1.5 mm, the tooth height H=18 mm and the tooth angle θ=20°. The first and last tooth show a radius on the external side of 9.0 mm.

For the leakage flow analysis, pressure values upstream and downstream were measured in order to calculate the pressure ratio β. The inlet total values were calculated starting from static values using the isentropic equations:

$$\frac{T_{1t}}{T_1} = 1 + \frac{\gamma - 1}{2} M_1^2 \tag{1}$$

$$\frac{P_{1t}}{P_1} = \left(1 + \frac{\gamma - 1}{2} M_1^2\right)^{\gamma/\gamma - 1} \tag{2}$$

where the inlet Mach value is calculated as

$$M_1 = \frac{c_1}{\sqrt{\gamma R T_1}} \tag{3}$$

and

$$c_1 = \frac{\dot{m}}{\rho B (H + cl)} \qquad \rho = \frac{P_1}{R T_1} \tag{4}$$

The flowfield visualization inside the clearance was performed by means of the Particle Image Velocimetry (PIV) technique that allows an indirect reconstruction of the velocity flowfield. Visualizations were made in adiabatic conditions, replicating selected fluid-dynamic conditions of the airstream in terms of Reynolds and reduced massflow. The seeding particles were injected into the airstream by the seeding generator at the inlet of the sample; in such a system a maximum of 4 Laskin nozzles were capable of generating small tracing particles of an average diameter of $1\mu m$ by means of compressed air. The air pressure reached a maximum of 2 bar and oil was used as a tracer.

The laser sheet was generated by a pulsating double cavity Nd-Yag NewWave® laser having an energy of 120 mJ per pulse at 532 nm; it has a repetition rate of 10 ns with a frequency of 15 Hz. All the double frames were acquired by a 1600x1200 pixels Dantec® FlowSense 2M camera with a 90 degrees optical access in between the clearance teeth. On the camera a 60mm Nikkor® macro lens was mounted with a narrow-band filter at 532 nm to avoid light diffusion or reflections. To improve the quality of the acquired images, teeth surfaces opposite the laser access were sprayed with a black dye to avoid laser reflections. Acquisitions were made with a 8.9 scale factor.

The test for the heat transfer analysis is started by switching on the electric heater, and the resulting conduction of heat into the test section walls has been numerically simulated on a finite element code using specified heat transfer coefficients of the magnitude and spatial variation expected for the experiments. For these conditions together with physical properties for acrylic plastic, the simulations show that the depth of heating in the wall over the expected test duration is less than the wall thickness. In addition, lateral conduction in the wall has a negligible effect on the local surface temperature response. At any surface point, the wall temperature can thus be represented by the classical one-dimensional response of a semi-infinite medium to the sudden step application of a convecting fluid at temperature $T_a w$:

$$(T - T_i)/(T_p - T_i) = 1 - exp(htc^2 \alpha \Theta / k^2) \cdot erfc(htc\sqrt{\alpha\Theta}/k) \quad (5)$$

However, in actual internal flow experiments, the wall surfaces will not experience a pure step change in air temperature because of the transient heating of the upstream plenum chamber and duct walls.

Nevertheless, equation (5) is a fundamental solution that can be used to represent the response to a superposed set of elemental steps as explained by Metzger and Bunker [7].

In the present experiments, air temperature is determined by the inlet and outlet thermocouple measurement. The variation with time is recorded and approximated by steps and the resulting superposed solution is solved for the local surface heat transfer coefficients, using observed local green peak times.

RESULTS

Comparison between measured and calculated leakage mass flow

Experimental data have been compared with calculated values from Sharrer's model as, among those analyzed, it is able to provide the best agreement.

Scharrer, as reported by Eldin [5], in order to develop his leakage model, used Neumann's equation as a base equation (6); the discharge coefficient is calculated using Chaplygin's formula, shown in equation (7) and the kinetic energy carry-over coefficient developed by Vermes, shown in equation (8).

$$\dot{m} = Cd \cdot \mu \cdot A \sqrt{\frac{P_i^2 - P_{i+1}^2}{RT}} \quad (6)$$

$$Cd = \frac{\pi}{\pi + 2 - 5\phi + 2\phi^2} \quad where \quad \phi = \left(\frac{P_i}{P_{i+1}}\right)^{\frac{\gamma-1}{\gamma}} - 1 \quad (7)$$

$$\mu = \sqrt{\frac{1}{1-\alpha}} \qquad where \qquad \alpha = \frac{8.52}{L/cl + 7.23} \quad (8)$$

In figure (3) the calculated and measured leakage flows versus β_{tot} are shown for all investigated configurations. The β_{tot} is defined as

$$\beta_{tot} = \frac{P_{1t}}{P_{14}} \quad (9)$$

In terms of mass flow rate, Sharrer's model produces an over-prediction for all cases. The errors decrease as the clearance increases. In fact, with clearance cl=6 mm the error is lower than 17% while for cl=3 mm it grows until 50%. One reason for this difference can be attributed to the different ratio cl/t that assumes in published works values lower than 1 but for this study varies from 1 to 4.

In figure (4) the pressure distribution measured for $\beta_{tot} = 2$ is plotted.

This figure shows a characteristic behavior at the seal inlet. A high decrease in static pressure is measured in the first cavity for all gaps compared with other constrictions. This difference increases with the increasing clearance according to the higher flow rate measured for a given β_{tot}. On the other hand, for the second cavity a very low pressure difference is shown for clearance cl=3 mm with even an increase in static pressure for clearances cl=4.5 mm and cl=6 mm. This result was obtained for all pressure ratios.

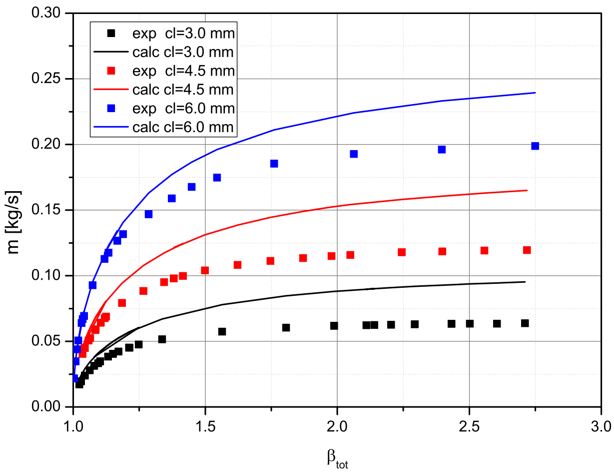

Figure 3. mass flow rate versus pressure ratio

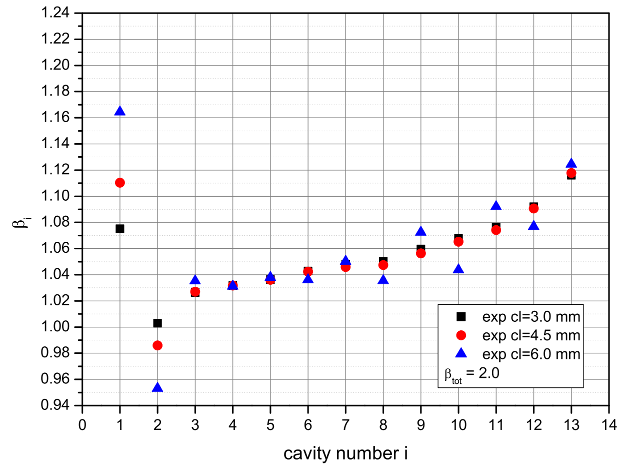

Figure 5. Pressure ratio of each constriction for β_{tot}=2

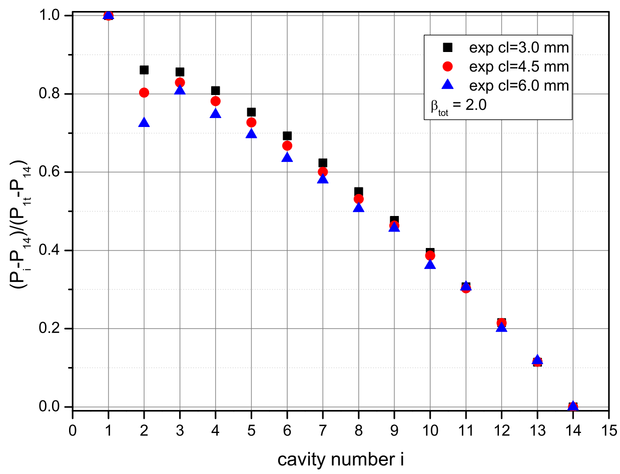

Figure 4. Pressure distribution for β_{tot}=2

This behavior was already shown by Zimmerman and Wolf [6] and Matthias and Willinger [11]. According to the explanation provided by Zimmerman and Wolf, the increase in static pressure is more evident for cl=6 mm than cl=4.5 mm. In fact, when increasing the clearance the aspect ratio of the cavity promotes the re-diffusion effect in this second cavity.

In figure (5) the total upstream to static downstream pressure ratios for each constriction is plotted for β_{tot}=2.0.

This figure shows that, excluding the first tooth, the efficiency in leakage reduction increases in the downstream direction. The first constriction is more effective at reducing the leakage flow than at least some (but not all) of the downstream constrictions due to the absence of the carry-over effect. According with this explanation, the pressure loss related to the first constriction increase with increasing of clearance for a given overall pressure ratio. The opposite trend is observed for the second constriction as explained before.

The range of total upstream to static downstream pressure ratio of the first tooth covers the range obtained for other constrictions during all tested conditions. Only the last constrictions in cases of higher overall pressure ratio β_{tot} gain a higher pressure ratio than the first one.

Moreover, this figure shows another interesting result. For clearance cl = 6 mm the pressure ratio of each constriction does not increase monotonically in the downstream direction. This trend is confirmed for both pressure ratio $\beta_{tot} = 1.5$ and $\beta_{tot} = 2.0$. This result is slightly visible for gap width cl = 4.5 mm while absent for cl = 3.0 mm.

This result can be explained by the influence of clearance on the flow field structure within the cavity with consequently different pressure losses. When the clearance is high the flow field in a cavity is affected by that of the near cavities. When the clearance decreases each cavity works separately from others. This explanation should be confirmed from above heat transfer and PIV investigation.

Leakage model description

In order to improve the capability for predicting leakage flow with a simple model, the experimental results are used to define a new discharge coefficient correlation. In fact, the continuity equation implies that the mass flow rate through each tooth is constant.

$$\dot{m}_1 = \dot{m}_2 = ... = \dot{m}_n = \dot{m} \tag{10}$$

where n is the number of teeth in the seal, $\dot{m}_1$ is the flow through the first tooth and $\dot{m}_n$ is the flow through the n-th tooth.

If the working fluid is assumed to be a perfect gas and the process is assumed to be isentropic, the mass flow rate for the subsonic case is given by the St. Venant equation (11) for the i-th constriction:

$$\dot{m}_{ideal} = \frac{P_{it} A}{\sqrt{R \cdot T}} \cdot \sqrt{\frac{2\gamma}{\gamma - 1} \left[\left(\frac{1}{\beta_i} \right)^{1/\gamma} - \left(\frac{1}{\beta_i} \right)^{\gamma + 1/\gamma} \right]} \quad (11)$$

where

$$\beta_i = \frac{P_{it}}{P_{i+1}} \quad (12)$$

This ideal flow rate was corrected to take into account the non-isentropic effects described previously, obtaining equation (13)

$$\dot{m} = Cd \cdot \mu \cdot \dot{m}_{ideal} \quad (13)$$

After each constriction, the isentropic pressure relationship (14) is applied to calculate the total pressure value using the Mach value calculated in the tooth throat.

$$\frac{P_{it}}{P_i} = \left(1 + \frac{\gamma - 1}{2} M^2 \right)^{\frac{\gamma}{\gamma - 1}} \quad (14)$$

According to the model suggested by Zimmerman and Wolf [6], the first constriction is treated separately. For this constriction the carry-over factor cannot be defined. Hence the first constriction must be modeled separately from others.

Effect of pressure ratio and geometry on discharge coefficient

Leakage behavior of the labyrinth seal is presented in a non dimensional form as discharge coefficient Cd. This parameter is defined for all constrictions as the ratio between measured and theoretical mass flow rate as given by equation (15).

$$Cd = \frac{\dot{m}}{\dot{m}_{theo}} \quad (15)$$

where the theoretical mass flow rate for first constriction is equal to the ideal mass flow rate

$$\dot{m}_{theo} = \dot{m}_{ideal} \quad (16)$$

while for other constrictions

$$\dot{m}_{theo} = \mu \cdot \dot{m}_{ideal} \quad (17)$$

where μ is calculated from equation 8. Thus the carry-over effect of each constriction is included in the theoretical mass flow rate.

The discharge coefficient obtained for the first tooth with all gaps is plotted versus pressure ratio in figure (6) and versus cl/t in figure (7).

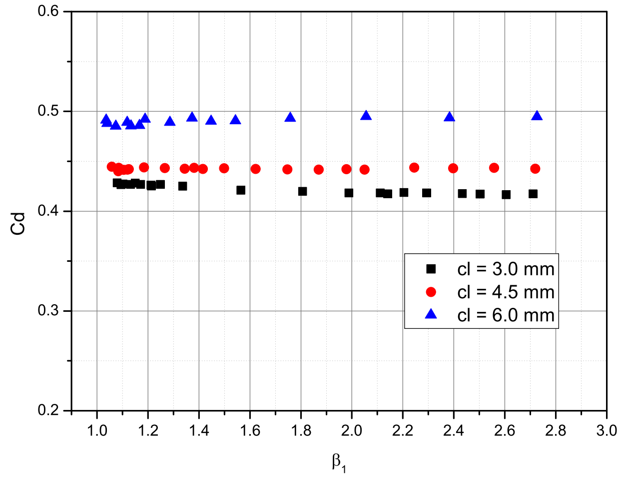

Figure 6. Cd versus β_1 for first constriction

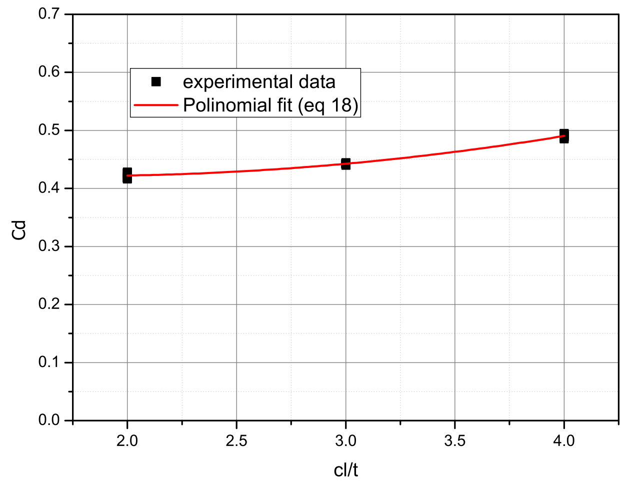

Figure 7. Cd versus cl/t for first constriction

As can be seen, for tested conditions the influence of the pressure ratio on discharge coefficient is negligible while its dependence on geometry is clearer. This is related to the high low tip tooth thickness compared with the clearance width with consequent dependencies on geometric parameters instead of pressure ratio. Only for gap cl=6 mm a slight increase in discharge coefficient is shown. The relationship between Cd and the ratio between clearance and tip tooth thickness, cl/t, has been correlated using a polynomial of order two and is shown in equation (18)

$$Cd = 0.464 - 0.049 \cdot (cl/t) + 0.014 \cdot (cl/t)^2 \qquad (18)$$

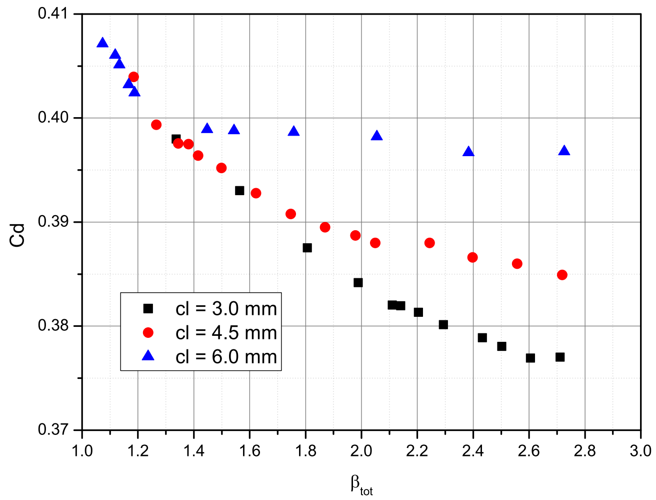

Figure 8. Cd versus β_{tot} for the rest of the seal constrictions

The discharge coefficient for other constrictions is, as explained in the previous section, different from these values because of the carry-over effect. In order to account for this effect the carry-over factor presented by Vermes (equation 8) was used to correct the ideal mass flow rate. The results obtained for all gaps are plotted versus pressure ratio in figure (8).

This figure demonstrates a very interesting result. The discharge coefficient starts from a value of approximately 0.41 for all geometries. Thus, the Verme's correlation is able to correctly take into account the geometry effect on correction factor. When β_{tot} increases the discharge coefficient decreases showing a different trend for each gap. Thus a power low was chosen for the discharge coefficient with the exponent based on the ratio L/cl. The new correlation is reported in equation (19)

$$Cd = 0.41 \cdot \beta_{tot}^{-0.00807 L/cl} \qquad (19)$$

Leakage flow and pressure distribution

The leakage model presented in this paper (equations 11 - 14) could be used with correlation (18) and (19) to calculate the leakage flow and pressure distribution along a straight through seal. A validation of this model was obtained comparing calculated values with experimental results obtained for a straight seal published by Vermes [4]. Figure 9 shows the capability of present leakage model to calculated the leakage flow for different seal clearance with an maximum error of 6.5%.

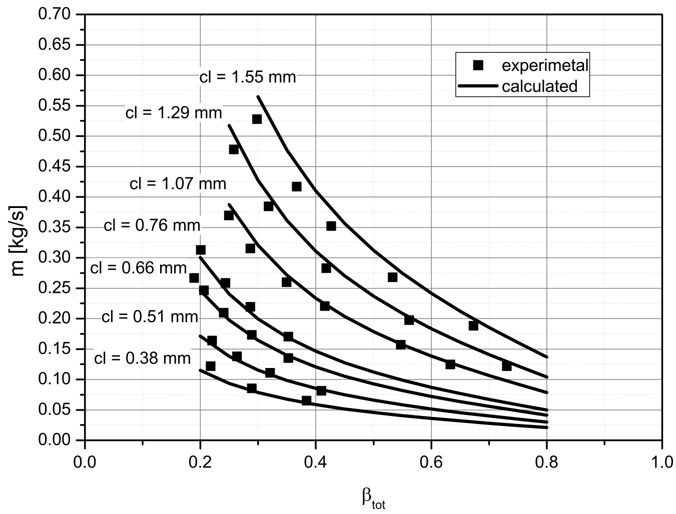

Figure 9. Comparison of calculated values and Vermes experimental results

Further validation is shown in figure 10 where calculated and experimental results are compared for two different seal geometries. A straight seal with the same dimension of previous (conf A) but with every sealing point removed (conf B) was tested, thus giving information on the performance of a labyrinth with 1/3 sealing points and pitch 3 times. This figure shows that the present correlations are able to correctly estimate the effect of pitch on leakage flow. Moreover an other interesting results is clear from this figure. In order to reduce the leakage flow, the pitch must be chosen in order to minimize the carry over factor.

In order to analyze the capability of the local model to predict the performance of each cavity, present experimental results are compared with calculated values. In fact, detailed results of pressure distribution within the seal are not present in literature.

The boundary conditions used for comparison are the measured inlet total pressure P_{1t} and outlet static pressure P_{14} of the seal. In figure (11) the calculated and measured mass flow rates are reported showing very good agreement. The calculated leakage values matched the experimental results with an error of less than 4% for all cases.

In figure(12) the pressure distribution calculated using the leakage model suggested in this paper is compared with the measured one for β_{tot}=2.0 for all gaps.

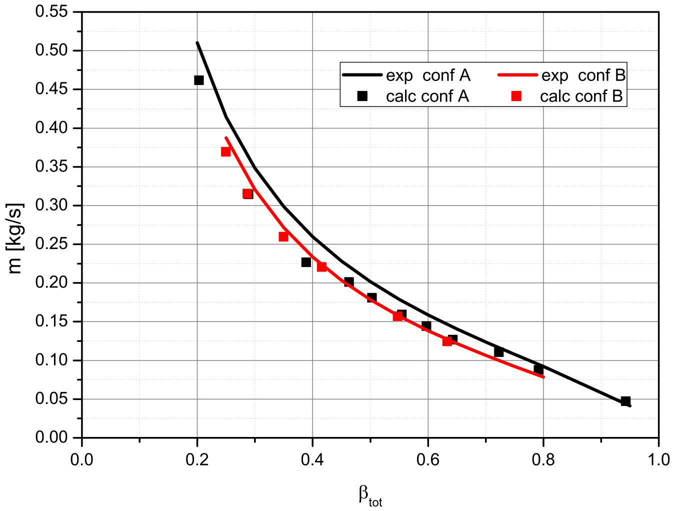

Figure 10. Effect of pitch on leakage flow

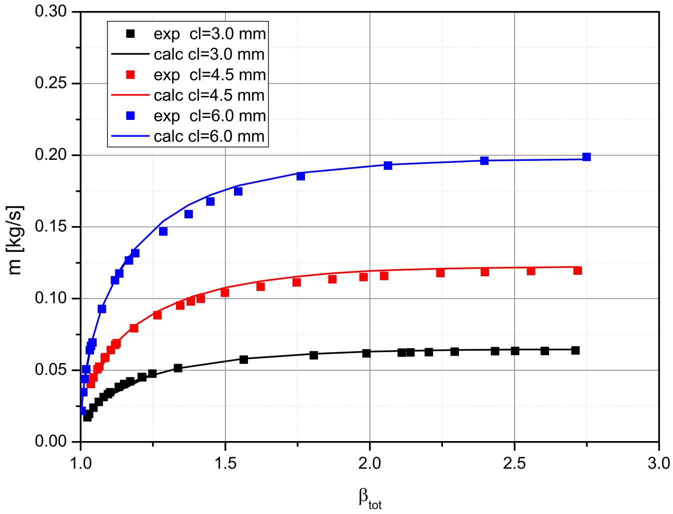

Figure 11. Mass flow rate versus pressure ratio

This figure shows a good prediction capability of pressure values using the model and correlations presented in this paper. Assuming the different modeling for the first tooth, the high pressure decrease related to this constriction is well predicted.

The use of the carry-over factor for all other teeth allows to predict the pressure distribution in agreement with the experimental data as well as the pressure recovery related to the rediffusion effect in the second cavity.

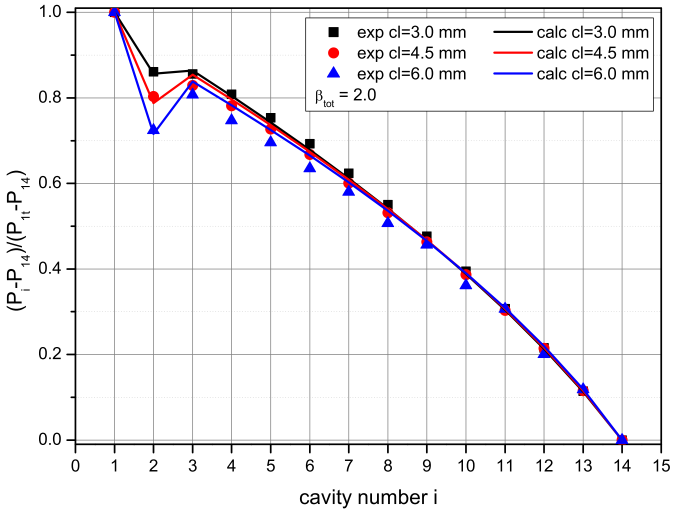

Figure 12. Calculated and experimental pressure distribution for cl=3.0 mm and β_{tot}=2.0

Flowfield Visualizations

Results of the PIV flowfield visualizations inside the clearance for all gaps and two different mass flow rates are presented, as summarized in Tab. 1; the investigation was performed among several consecutive teeth, so to limit the length of this section only selected results are discussed.

gap [mm]	6.0	4.5	3.0
Minimum mass flow rate [kg/s]	0.02	0.02	0.04
Maximum mass flow rate [kg/s]	0.062	0.062	0.124

Table 1. Investigated flow conditions

Before analyzing vector maps, some general flowfield trends arisen from measurements have to be pointed out. In each gap, for both the minimum and maximum massflow rates, no uniform behavior between the teeth was measured due to a different interaction of the main airstream with obstacles, that is affected by unsteady flow structures generated by teeth tip: vortices that separate from obstacles are swept away by the main airstream interacting with downstream teeth depending on the investigated massflow rate. Due to the highly unsteady behavior of such phenomena, flowfield visualizations were performed in several tests reproducing similar conditions and repeatability of measurements was successfully checked.

Let us now focus on the detailed description of selected cavities vector fields; first of all an example of the vector map upstream from the first clearance tooth is shown in Fig. 13(a) for cl=4.5mm, presenting the axial velocity (U) plot as well in Fig. 13(b). At the entrance of the clearance the airstream is aligned with the smooth surface because the airstream flows from the settling chamber inside the inlet smooth duct (Fig. 1). The first tooth has a large fillet radius at the inlet of the labyrinth seal to avoid flow recirculation; at the same time it is responsible for the flow acceleration from the free smooth duct to the small clearance gap: as shown in Fig. 13(b), the airstream accelerates in the region corresponding to the fillet radius, with an increase of velocity radial component as well, as depicted in Fig.13(a), where velocity magnitude is shown.

The steep height constriction generates a flow separation from tooth tip, reducing the effective passage area in the first gap with a maximum flow velocity measured near the smooth surface.

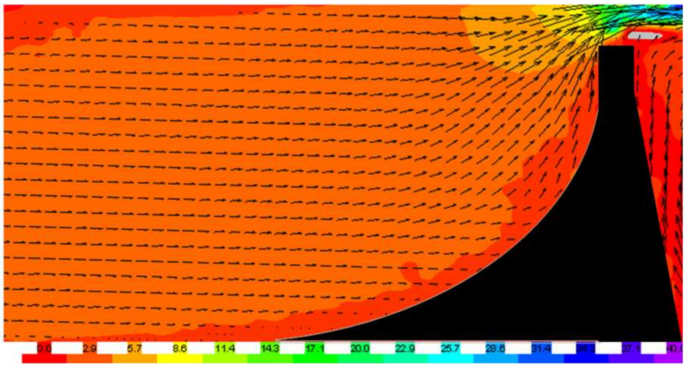

(a) Vector velocity field - $\sqrt{U^2+V^2}$ - m/s

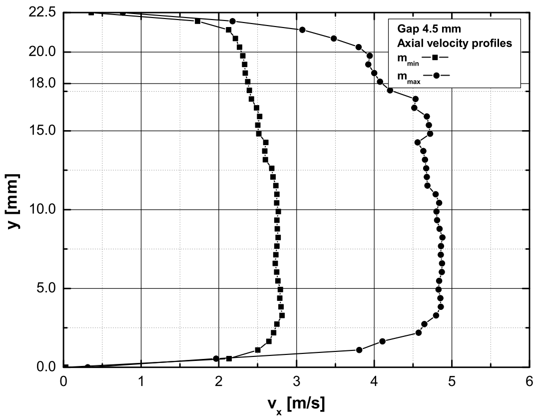

(b) Axial velocity U profile - m/s

Figure 13. Test sample inlet - GAP 4.5mm - maximum mass flow rate

The height reduction due to clearance teeth and the interaction of unsteady flow structures with consecutive obstacles alter the velocity profile near the smooth surface and within the cavity; to better clarify the first effect, velocity profiles for cl=4.5mm, referred to the middle section of the cavity, are presented for m_{min} and m_{max} in Fig. 14 for the first two cavities. In the region above teeth tip ($18 < y < 22.5$mm), the maximum axial velocity U is measured near the smooth surface for m_{max}, while with a lower massflow rate the maximum axial velocity is at about $y = 21mm$. This effect is mainly ascribable to the different velocity of the airstream discharged from tooth gap: with a higher massflow rate, the airstream has a higher momentum and jet length is higher.

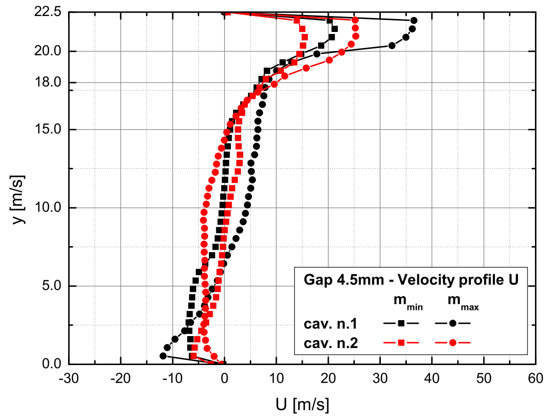

Figure 14. Cavity n.1 and n.2 axial velocity profile - U - $[m/s]$

As already stated, the airstream massflow rate and gap width are also responsible for a different flowfield behavior, as shown in Fig. 15. Referring to cl=3mm, the recirculation core in the first cavity for m_{min} is displaced near the first tooth as a consequence of the interaction of the airstream with the second tooth surface: near tip the flow is diverted inside the cavity, where it creates the recirculation, and through the second gap. With cl=4.5mm, the recirculating area is located upstream from the second tooth; in this case the massflow rate is halved and hence the interaction of the airstream with the second tooth is altered.

By comparing the results for m_{min} and m_{max}, the center of recirculating area is shifted in both cavity for cl=3 and 4.5mm; with a greater gap thickness, vortices, that are initially located upstream and downstream from the second tooth, moves towards the inlet of the clearance and the third tooth respectively. In the case of the minimum gap thickness, vortices become centered on the cavities.

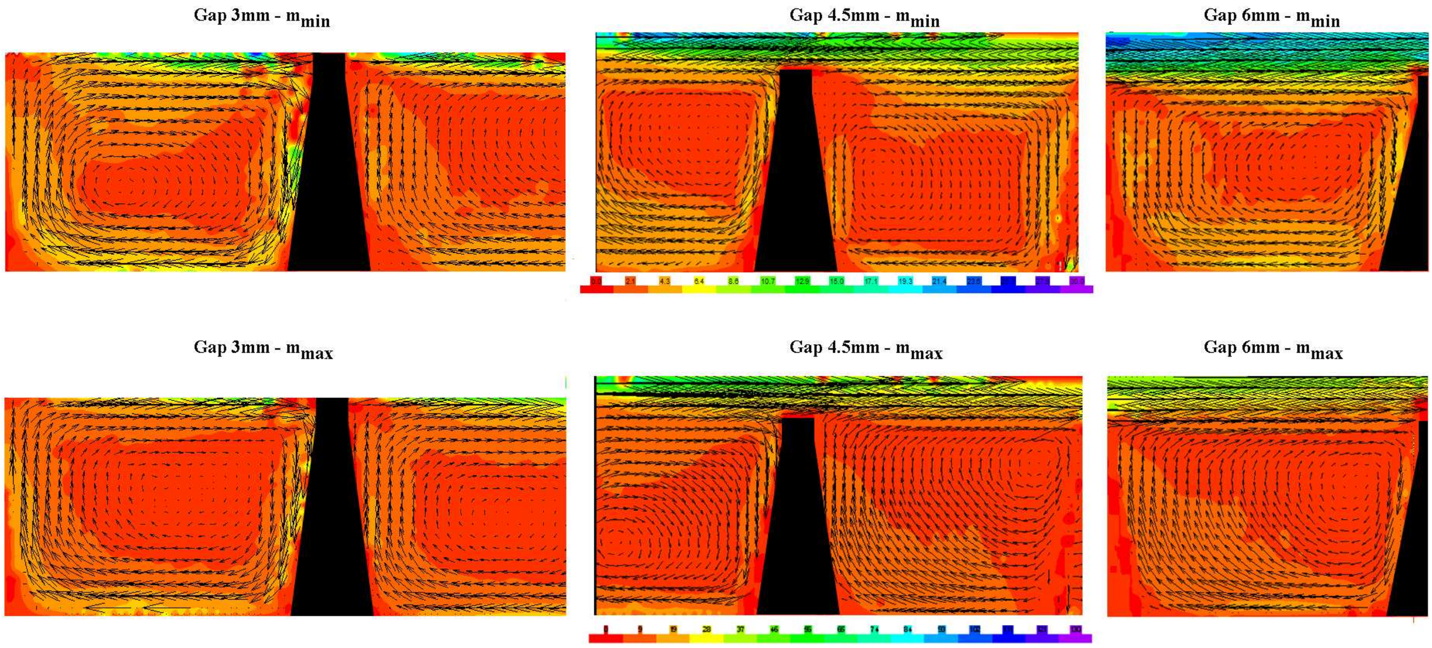

Figure 15. Cavity n.1 and n.2 vector flowfield - $\sqrt{U^2+V^2}$ - $[m/s]$

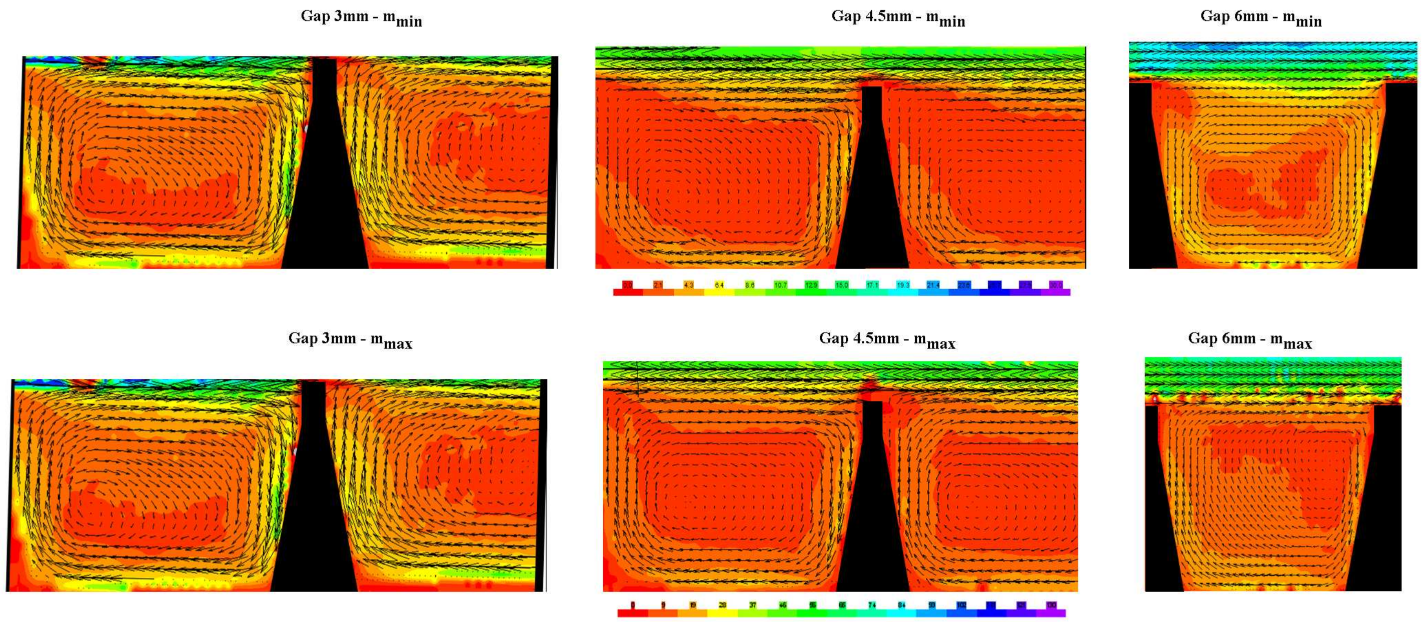

Figure 16. Cavity n.7 and n.8 vector flowfield - $\sqrt{U^2+V^2}$ - $[m/s]$

For cl=6mm the vector map is presented for cavity n.2, showing that the flowfield for different mass flow rates is similar. In this case, the higher clearance gap allows to reduce the interaction between the airstream and teeth surface.

Afterwards, the flowfield visualization is presented within cavities n.7 and 8 in Figure 16: as a general remark, flow structures arising for cl=3 and 4.5mm are similar up to the clearance outlet, regardless of air velocity.

Heat transfer

The influence of seal clearance and Reynolds number on local transfer coefficient will be presented in this section. Four Reynolds numbers were tested for each configuration. The hydraulic diameter of the labyrinth gap (2·cl) represents the characteristic length scale for the Reynolds number and Nusselt number defined as:

$$Re = \frac{2\dot{m}}{\mu B} \tag{20}$$

$$Nu = \frac{htc\ 2\ cl}{k} \tag{21}$$

The local Nusselt numbers are presented in figures 17-20 for the stator and rotor sides of all gaps. Each curve represents a distribution of the local Nusselt number for a given Reynolds number. The effects of the Reynolds number and gap width on the Nusselt number profiles are studied in the present paper.

For gap cl=6 mm, at the top wall (figure 17) the local Nusselt number increases with an increasing Reynolds number.

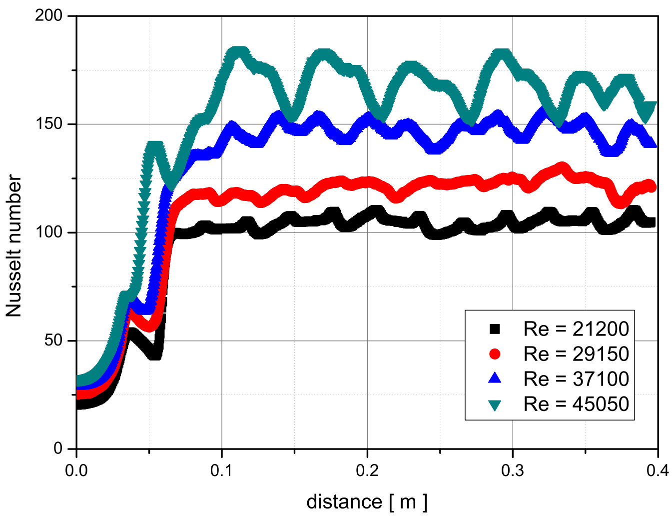

Figure 17. Local Nusselt numbers at the top side, gap cl=6 mm

For all cases a large increase of Nusselt numbers at the seal inlet can be observed. This is related to the increase in turbulence due to the presence of the tooth and the lower area available for leakage flow that produces an increase in mean velocity. After the first constriction a decrease of Nusselt numbers is observed for $Re \approx 21000$. For $Re \approx 29000$ and $Re \approx 37000$ this decrease is less marked while for $Re \approx 45000$ it is not shown but is present after the second constriction. This can be justified with an increase in the mass velocity ratio that produces a different flow field as shown from PIV investigation.

For $Re \approx 21000$, the Nusselt numbers assume almost constant values after the second constriction. A low increase is shown in correspondence to each constriction with a subsequent decrease in the downstream cavity around the mean value. Increasing the Reynolds number, the position where the peak is reached moves forward and a larger difference in Nusselt numbers is shown from the average value for each constriction. For $Re \approx 45000$ these differences show clearly that the flow field within the cavities of the seal is different. In particular the same flow field is shown for each pair of cavities in the middle of the seal. Even if it is less clear, the same behavior is shown for $Re \approx 37000$ but for different cavities. Therefore the qualitative distribution of the local Nusselt numbers at the top side exhibits definite dependence on the Reynolds number.

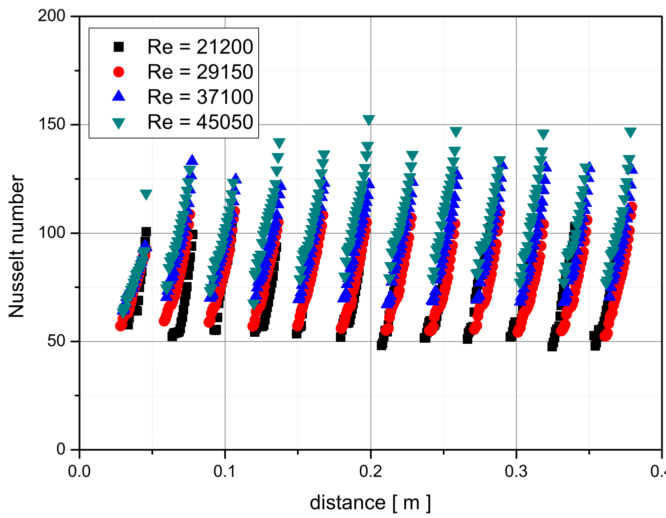

Figure 18. Local Nusselt numbers at the bottom side, gap cl=6 mm

In figure 18 results obtained for the bottom side with gap cl=6 mm are shown. Again, the values of the local Nusselt numbers increase when the Reynolds number increase. Compared to the top side, larger differences in the distribution of the local Nusselt number are shown for a given Reynolds number within each seal cavity. This strong increase is related to the recirculation that settles in after the teeth. The shape of the distributions of the local Nusselt numbers for the bottom side with gaps cl=4.5 mm and cl=3 mm is very similar to this obtained for gap cl=6 mm and then it is not showed in this paper.

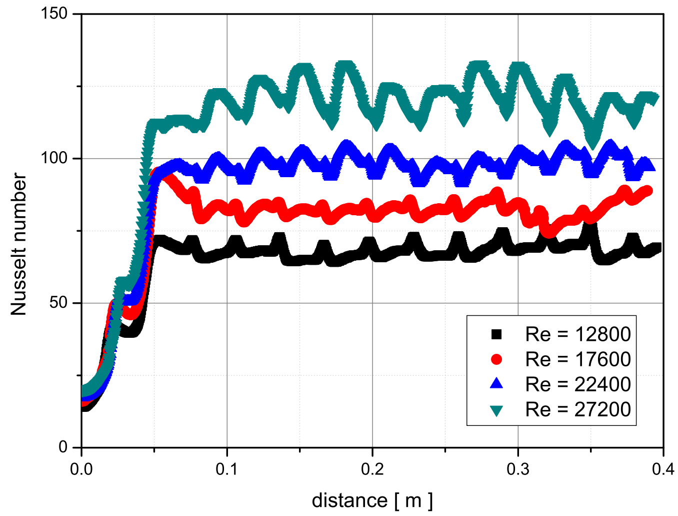

Figure 19. Local Nusselt numbers at the bottom side, gap cl=4.5 mm

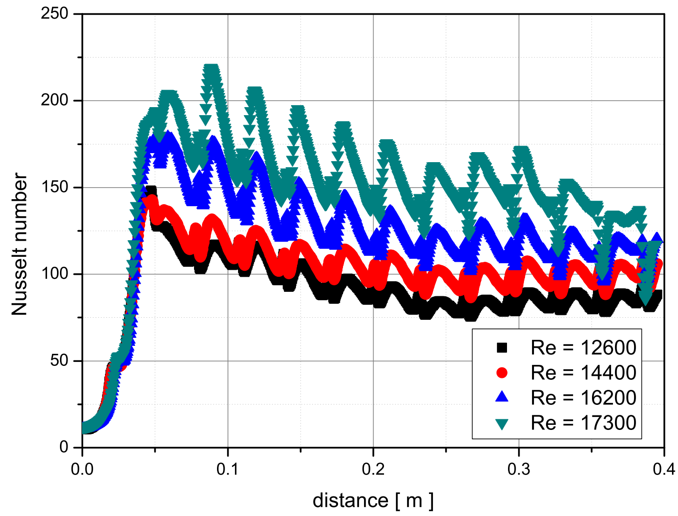

Figure 20. Local Nusselt numbers at the top side, gap cl=3 mm

Similar results have been obtained for the top side with gap cl=4.5 mm (Figure 19). The main difference for this gap with respect to the previous one is that the effects of vortex are less evident for this case. According to the results obtained from the PIV investigation for this gap, the flow field within each seal cavity becomes more similar to others. Hence, the Nusselt numbers distribution is more similar for all cavities. Starting from Re=17600 with this gap, the distribution of Nusselt numbers shows a local phenomena near the constrictions. A first increase is measured near the teeth tip with a second increase downstream. The former is related to the local acceleration because of the presence of constriction, the latter is related to the vortex that detaches after the tip teeth. With lower gap width and higher mass flow rate both effects become more visible in the heat transfer distribution. The results obtained with this gap show that the second increase becomes more important than the first with an increasing Reynolds number.

As shown in Figure 20, the qualitative distribution of the local Nusselt numbers at the top side is completely different with gap cl=3 mm. After the first constriction an increase in values is measured for all Reynolds numbers. After the second tooth, the trend shows an initial decrease and becomes constant in the second part of the seal for all Reynolds numbers except Re=17300. For this case the highest value of Nusselt numbers is measured downstream from the third tooth. For all cases the presence of two peaks of heat transfer after each constriction is clearly visible. The width of these increases is comparable for lower Reynolds numbers while for higher ones the second peak becomes greater than the first as shown by gap cl=4.5 mm as well.

CONCLUSIONS

A comprehensive experimental investigation on a straight through labyrinth seal is presented in this paper. Influence of the clearance gap width and pressure ratio on discharge coefficient, heat transfer and flow field within the seal has been analyzed.

In order to correctly predict the leakage flow for this seal configuration a new leakage model has been proposed. The different treatment of the first constriction and the new correlations for discharge coefficient allow to correctly estimate both pressure distribution and leakage mass flow rate for all gap widths investigated with an error of less than 4%. The pressure ratio of each constriction increases in the forward direction but shows a non monothonic trend for higher clearance. This different behavior of each cavity is confirmed by PIV investigation and heat transfer analysis and decreases with a decreasing clearance width.

Flowfield visualizations, made by means of the PIV technique, showed a non uniform flowfield trend inside each gap; in gaps 3 and 4.5 mm coherent vector field were measured comparing the lower and higher massflow rates.

As expected, the Nusselt numbers increase when the Reynolds number increases. The qualitative distribution of the local Nusselt numbers at the top side exhibits definite dependence on the gap width. At the inlet a strong increase in Nusselt numbers is measured. Depending on the clearance, a mean constant value is gained starting from second or third constriction except for clearance cl=3.0mm which shows a decrease of the distribution of Nusselt numbers. Local variations are due to the presence of constriction and vortex that detaches after the tip teeth. Both gap width and Reynolds number affect these variations.

ACKNOWLEDGMENT

The authors would like to thank Ansaldo Energia for giving their permission to publish this work.

REFERENCES

[1] Egli, A., 1935. "The leakage of steam through labyrinth seals". *Trans. ASME*, **57**, pp. pp 115–122.

[2] Martin, H. M., 1908. "Labyrinth packings". *Engineering*, pp. pp 35–36.

[3] Hodkinson, B., 1939. "Estimation of the leakage through a labyrinth gland". *Proceedings of the Institution of Mechanical Engineers*, **141**, pp. pp 283–288.

[4] Vermes, G., 1961. "A fluid mechanics approach to the labyrinth seal leakage problem". *Trans. ASME - Journal of Engineering for Power*, **83 (2)**, pp. pp 161–169.

[5] Eldin, A. M. G., 2007. "Leakage and rotordynamic effects of pocket damper seals and see-through labyrinth seals". *PhD Thesis, Texas A&M University*, **57**.

[6] Zimmermann, H., and Wolff, K. H., 1987. "Comparison between empirical and numerical labyrinth flow correlations". *ASME Paper*(87-GT-86).

[7] Metzger, D. E., and Bunker, R. S., 1985. "Heat transfer for flow through simulated labyrinth seals". *presented at the Symposium on Transport Phenomena in Rotating Machinery*. Honolulu, USA.

[8] Willenborg, K., Kim, S., and Wittig, S., 2001. "Effect of reynolds number and pressure ratio on leakage loss and heat transfer in a stepped labyrinth seal". *ASME J. Turbomach.*, **123**, pp. pp 815–822.

[9] Willenborg, K., Schramm, V., Kim, S., and Wittig, S., 2002. "Influence of a honeycomb facing on the heat transfer in a stepped labyrinth seal". *ASME J. Eng. Gas Turbines Power*, **124**, pp. pp 133–139.

[10] Waschka, W., Wittig, S., and Kim, S., 1992. "Influence of high rotational speeds on the heat transfer and discharge coefficients in labyrinth seals". *ASME J. Turbomach.*, **114**, pp. pp 462–468.

[11] Matthias, A., and Willinger, R., 2009. "Influence of rotation and eccentricity on labyrinth seal leakage". *Proceedings of the 8° ETC*, pp. pp 1355–1363.